Chaos in coherence modulation: bifurcations of an oscillator generating optical delay fluctuations

Laurent Larger*, Min Won Lee*, Jean-Pierre Goedgebuer*,

Thomas Erneux** and Wilhelm Elflein*

* Laboratoire d'Optique P.M. Duffieux, UMR 6603 CNRS,

Institut des Microtechniques de Franche-Comté, FRW 0067

CNRS, UFR Sciences et Techniques, Université de

Franche-Comté, Route de Gray, 25030 Besançon cedex, France

** Groupe d'Optique Non Linéaire théorique, Université Libre

de Bruxelles, Campus Plaine, C.P. 231, 1050 Bruxelles, Belgium

laurent.larger@univ-fcomte.fr

A new chaos generator is described, which produces chaotic fluctuations of the optical path difference in a coherence modulator driven electrically by a nonlinear delayed feedback loop. Numerical simulations and experimental results are reported. A closed branch of periodic solutions bounded by a forward and a reverse Hopf bifurcation is observed for the first time for this type of nonlinear dynamical system.

OCIS codes: 190.3100, 030.1670, 130.0250

1. Introduction

Chaotic processes can be observed in various domains such as economy, biology, thermodynamics, mechanics and optics. One of the first optical systems for chaos generation was reported by Ikeda,[1] who described a set–up consisting of a ring cavity with a nonlinear feedback. Other optical systems have been investigated, where chaos has been observed in the behavior of laser spatial patterns beams, laser polarization states,[2] laser wavelength,[3,4] and laser intensity which is the case mostly studied.[5–7] In this paper, we report a chaos generator based on an unusual dynamical variable, the optical path difference (OPD) in a coherence modulation system. The system is realized from a Mach–Zehnder (MZ) coherence modulator powered by a short coherence source and driven with a nonlinear feedback loop containing a second MZ interferometer and a delay line. The dynamics of this system are shown to be ruled by a first order nonlinear delay differential equation exhibiting interesting bifurcation diagrams. In addition to the well known cascade of period doubling bifurcations leading to chaos, we find closed branches of periodic solutions. Such a bifurcation sequence was reported on dynamical systems of different types,[8] but was never observed in previous experiments based on nonlinear delayed dynamics like the one reported in the present article.

The paper is organized as follows. In Section 2 we briefly recall the basic principles of coherence modulation and derive the nonlinearity that is used to generate a chaotic coherence modulated light beam. The experimental setup and its operating principle are described in Section 3. In Section 4, numerical simulations are compared with experiments. Finally, we explain in Section 5 why closed branches of periodic solutions are possible for our device.

2. Coherence modulation

When looking for optical devices capable of producing chaotic outputs, it is natural to consider nonlinearities induced by the optical power. Such nonlinearities often feature instabilities that require

an accurate control of the laser pulses used. The nonlinearity (NL) used in the setup described in this paper is however generated via the modulation transfer function (MTF) of a coherence modulation system. Coherence modulation of light has been widely investigated theoretically and experimentally during the last years for applications to sensors,[9] telecommunication systems[10] and secure communications.[11] We refer the reader to Ref.[12] for a detailed analysis of coherence modulation from considerations on the temporal coherence degree of light. A basic system for coherence modulation consists of a broadband optical source (power spectrum $P(\sigma)$) and a pair of interferometers, with optical path-differences (OPD) D_1 and D_{20}, respectively, that are greater than the coherence length $L_C = 1/\Delta\sigma$ of the source ($\Delta\sigma$ is the linewidth at e^{-1} of the source expressed in wavenumber $\sigma = 1/\lambda$; D_1 is assumed to be an OPD that can be varied electro-optically while D_{20} is constant). The light intensity I at the second interferometer output is given by[10]

$$I = \frac{\alpha P_0}{4}\left[1 + \frac{1}{2}\Gamma(D_1 - D_{20})\cos\left[2\pi\sigma_0(D_1 - D_{20})\right]\right] \tag{1}$$

where α is related to the optical losses in the system, P_0 is the optical power of the source and σ_0 is the center wavenumber. The function $\Gamma(.)$ describes the temporal coherence degree of the source, and is given by the cosine Fourier Transform of the power spectrum $P(\sigma)$ of the source i.e.,

$$\Gamma(D) = \int_{-\infty}^{+\infty} P(\sigma)\cos(2\pi\sigma D)\, d\sigma. \tag{2}$$

If the source exhibits a Gaussian power spectrum of the form

$P(\sigma) = P_0 \dfrac{2}{\Delta\sigma\sqrt{\pi}} \exp\left\{-\dfrac{4}{\Delta\sigma^2}\,\sigma^2\right\}$,

the temporal coherence degree is

$\Gamma(D) = P_0 \exp\left(\dfrac{-\pi^2 D^2}{4L_C^2}\right)$

and Eq. (1) becomes

$$I = \frac{\alpha P_0}{4}\left[1 + \frac{1}{2}\exp\left\{\frac{-\pi^2(D_1 - D_{20})^2}{4L_C^2}\right\}\cos\{2\pi\sigma_0(D_1 - D_{20})\}\right] \quad (3)$$

Eq. (1) or (3) considerably simplify if we now assume that the OPD D_{20} of the second interferometer coincides with D_1 to within a fraction of the coherence length. Then, the term $\Gamma(D_1 - D_{20})$ in Eq. (1) or the exponential in Eq. (3) becomes unity. This means that the two cascaded interferometers admit a modulation transfer function that is a cosine function vs D_1, with a 50 % modulation depth:

$$MTF = \frac{1}{4}\left[1 + \frac{1}{2}\cos\{2\pi\sigma_0(D_1 - D_{20})\}\right] \quad (4)$$

Such a nonlinear dependence of the MTF vs D_1 forms the core of our experiments. For the system to operate as a chaotic oscillator it is known that the nonlinearity should exhibit at least one minimum or one maximum. This condition can be easily met with a suitable choice of the OPD D_1 as explained in the following section.

3. Experimental set–up

The experimental set–up is shown in Fig. 1. Specifically, the chaotic oscillator consists of:

- a pigtailed superluminescent diode SLD with an output power $P_0 = 650\ \mu W$ and a central wavenumber $\sigma_0 = 0.78\ \mu m$ ($\lambda_0 = 1.28\ \mu m$). The power-spectrum $P(\sigma)$ of the source is approximately Gaussian, with a linewidth $\Delta\sigma = 21\times10^{-3}\ \mu m^{-1}$ ($\Delta\lambda = 35\ nm$) at e^{-1}, yielding a coherence length $L_C \simeq 47\ \mu m$

- two $LiNbO_3 : Ti$ integrated MZ modulators (MZ_1 and MZ_2), which generate the nonlinear MTF described in Eq. (4). The total optical power losses are $-12\ dB$. Those MZ modulators were fabricated specifically to feature unbalanced branches with large OPDs $D_{10} = D_{20} = 260\ \mu m$, when no voltage is applied to the electrodes. The fabrication process used was described in[9] for other

purposes. When applying a voltage V on MZ_1, the OPD becomes $D_1 = D_{10} + \delta D$ (with $\delta D << L_C$), where $\delta D = V/2\sigma_0 V_\pi$ is the electrically-induced optical path-difference, and $V_\pi = 4.3\ V$ the half-wave voltage.

From Eq. (3) with the exponential equal to one, the optical intensity $I(V)$ at the output of MZ_2 can then be rewritten as:

$$I(V) = \frac{\alpha P_0}{2}\left[1 + \frac{1}{2}\cos\left(\Phi + \pi\frac{V}{V_\pi}\right)\right] \tag{5}$$

where $\Phi = 2\pi\sigma_0(D_{10} - D_{20})$. The other elements of our experimental set–up are

- a fiber polarizer placed between the modulators

- a delay line formed by a 22 km-long fiber, yielding a time delay $T = 110\ \mu s$.

- a photodetector PD, which converts the optical intensity $I(V)$ at the output of MZ_2 into a feedback voltage with a conversion factor $K = 1.5\ V/\mu W$, and a cut-off frequency $f_c = 25\ kHz$, yielding a loop response time $\tau = 1/2\pi f_c \simeq 6.4\ \mu s$. The dynamics of the feedback voltage $V(t)$ are then ruled by a first order delay differential equation given by:

$$V + \tau\frac{dV}{dt} = K\, I[V(t-T)] \tag{6}$$

Finally, the fluctuations δD of the OPD D_1 around its central value D_{10} satisfy the following delay differential equation (DDE):

$$\delta D(t) + \tau\frac{d[\delta D]}{dt}(t) = \beta_{\delta D}\left[1 + \frac{1}{2}\cos\{\Phi + 2\pi\sigma_0\delta D(t-T)\}\right] \tag{7}$$

where $\beta_{\delta D} = \alpha K P_0/2\sigma_0 V_\pi$ is the bifurcation parameter. Note that the parameter $\Phi = 2\pi\sigma_0(D_{10} - D_{20}) = \pi V_0/V_\pi$ can be varied electrically by means of a bias voltage V_0 applied to MZ_1. The bifurcation parameter $\beta_{\delta D}$ can be varied via the photodetector gain K.

In the next section, we report numerical simulations for two different values 0 and π of the parameter Φ. These values can be easily adjusted experimentally, and are used to compare the theoretical and experimental results.

4. Bifurcations and routes to chaos

A. Numerical simulations of the dynamics

Equation (7) can be further simplified if we introduce the normalized variables x and θ defined by $x = 2\pi\sigma_0(\delta D)$ and $\theta = t/T$. In terms of these new variables, Eq. (7) becomes,

$$x(\theta) + \eta\frac{dx}{d\theta}(\theta) = \beta\left[1 + \frac{1}{2}\cos\{x(\theta - 1) + \Phi\}\right] = f[x(\theta - 1)] \tag{8}$$

where the new parameters η and β are given by $\eta = \tau/T$, and $\beta = \pi\alpha K\, P_0/V_\pi$. The simulations were carried out using the 4^{th} order Runge-Kutta numerical integration with values of the normalized bifurcation parameter β ranging from 0 to 10.

We used 400 samples per time delay T, yielding an integration step of $d\theta = 2.5 \times 10^{-3}$. The normalized time response was $\eta \simeq 5 \times 10^{-2}$. Note that the ratio $T/\tau = 1/\eta$ is about 20, which is a value high enough to observe Ikeda's instabilities and chaotic behaviors.[1] Figures 3a and 3b show the bifurcation diagrams for $\Phi = 0$ and π, respectively. The values of the variable x obtained from the numerical integration of Eq. (8) are stored to compute the probability density function (PDF) of the dynamics for each value of β. The PDF is displayed along the vertical axis with different gray levels using a 600 sampled values of x in the range $[0.5; 10]$. Along the horizontal axis, we also sampled 600 values of β between 0 and 10. Such a process yields bifurcation diagrams close to that observed experimentally when using an oscilloscope.

The bifurcation diagrams shown in Fig. 3 illustrate two different routes to chaos as we increase β. For $\Phi = 0$ (Fig. 3a) a period doubling cascade starts at $\beta = \beta_c \simeq 2.083$. Note that the next

bifurcation (at $\beta_c \simeq 5.041$) changes the period-2 cycle back to a stable steady-state, instead of the period-4 usually reported for similar time-delayed dynamical systems.[1,4,13] We call this specific diagram an *"eye bifurcation cascade"*. A third bifurcation is then observed for $\beta \simeq 6.591$, with a strong jump from a steady-state to chaotic oscillations, yielding a crisis.

For $\Phi = \pi$ (Fig. 3b), increasing β from zero, a period doubling cascade starts, for $\beta \simeq 2.889$ with a transition from a steady-state to a period-2 cycle. The cascade then continues at $\beta \simeq 3.548$ with the bifurcation of period-2 to period-4. However, if β is further increased ($\beta > 3.548$), the cascade stops and a reverse bifurcation scenario occurs, which changes the period-4 into a period-2 at $\beta \simeq 4.459$. The period-2 cycle jumps suddenly if $\beta \simeq 4.851$, yielding another period-2 regime located on another attractor (with different amplitudes). From that period-2 regime, the usual period-doubling cascade is observed numerically, and leads to an accumulation point. Chaotic regimes start at that point, and finally yield to a fully-developed chaos for $\beta \geq 5.195$, through a reverse cascade scenario.

B. Experimental results

The behavior of MZ_1 as a coherence-modulator was first checked experimentally with no feedback loop. The light from MZ_1-output was analyzed using a Michelson interferometer with a variable OPD Δ (the Michelson interferometer used to test the device is not represented in Fig. 1). The interference pattern thus obtained at the output of the Michelson interferometer is shown in Fig. 2a as Δ is varied from $-350\ \mu m$ to $+350\ \mu m$. The location of the two side fringe patterns (shown in Fig. 2b) at $\Delta = \pm 260\ \mu m$ gives the value of the OPD D_{10} of MZ_1 (Note that the fringe envelope, which is related to the temporal coherence degree Γ, is Gaussian).

We then measured the experimental MTF of the system. This was performed by adjusting the OPD Δ of the Michelson interferometer at $\Delta = D_{10} = 260\ \mu m$ and applying a sine voltage V with a peak-to-peak amplitude of $21\ V$. The intensity modulation thus obtained at the Michelson output

is shown in Fig. 2c and represents the MTF described by Eq. (4).

Finally, the system was operated with the feedback loop, as shown in Fig. 1. In the experiments, the amplitude of the voltage V fed back to the electrodes of MZ_1 was adjusted to be greater than V_π, in order to operate the system with at least one extremum in the NL-function. This was achieved by amplifying the voltage V with a gain K varying between 0 and 20 dB. For $K = 20$ dB, the amplitude of voltage V was 21 V. The system then operated with the NL-function featuring 4 extrema, as already shown in Fig. 2c. Under these conditions, β can be varied between 0 to 10. Additionally, a bias voltage V_0 was added to the feedback voltage $V(t)$ of MZ_1, in order to fix the parameter Φ to 0 ($V_0 = 0$ V) or π ($V_0 = 4.3$ V).

Figure 4 shows the experimental bifurcation diagrams obtained for $\Phi = 0$ and $\Phi = \pi$. For $\Phi = 0$ (Fig. 4a), the bifurcation sequence (*fixed point*$\rightarrow$ *period-2*$\rightarrow$ *fixed point*$\rightarrow$ *chaos*) occurs at $\beta_c = 2.07; 5.3; 6.69$, respectively. For $\Phi = \pi$ (Fig. 4b), the bifurcation sequence (*fixed point*$\rightarrow$ *period-2*$\rightarrow$ *period-4*$\rightarrow$ *period-2*) occurs at $\beta_c = 2.71; 3.55; 4.54; 5.13$, respectively. Those values are in good agreement with those predicted from the numerical bifurcation diagrams shown in Fig. 3a and 3b.

5. Analysis of the *"eye bifurcation cascade"*

In this section, we explain why the specific *"eye bifurcation cascade"* as shown in Fig. 3a or Fig. 4a was not observed in earlier experiments based on similar dynamics. Nevertheless works[8] on electronic and all optical driven nonlinear oscillators have previously reported reported such so–called antimonotonic bifurcation diagrams. Specifically, we analyze the stability of the steady state for a general class of first order DDE, determine the Hopf bifurcation conditions, and then apply our results for a sine-type nonlinearity which is often the case in optics.

A. Linear stability analysis for nonlinear DDE*s*

An explanation of the bifurcation sequence shown in Figs 3a and 4a is obtained by analyzing the linear stability of the steady states of Eq. (8). Equation (8) is of the form

$$\eta \frac{dx}{d\theta}(\theta) = -x(\theta) + f(\beta, x(\theta - 1)) \tag{9}$$

where β is the bifurcation parameter. The steady state solutions, $x = x_s$ are then the root of the following equation

$$0 = -x_s + f(\beta, x_s). \tag{10}$$

Introducing the small deviation $u = x - x_s$, the linearized problem is given by

$$\eta \frac{du}{d\theta}(\theta) = -u(\theta) + f_x(\beta, x_s)u(\theta - 1) \tag{11}$$

and admits the solution $u = c\exp(\sigma\theta)$ where the growth rate σ satisfies the transcendental equation

$$\eta\sigma = -1 + f_x(\beta, x_s)\exp(-\sigma). \tag{12}$$

We next assume that a Hopf bifurcation is possible, characterized by a change of stability expressed by σ purely imaginary, $x_s = x_c$ and $\beta = \beta_c$. Substituting $\sigma = i\omega$ into Eq. (12) gives particular relations between ω, β_c and x_c at the Hopf point. We wish to determine the stability properties of the steady state in the vicinity of the Hopf bifurcation point. That problem is solved if we know the sign of $\Re(\sigma)$ given by Eq. (12), which is to be evaluated along the steady state curve in the vicinity of the Hopf point. To this end, we first determine how $x_s - x_c$ changes as $\beta - \beta_c$ is changed. Introducing the small deviation $B = \beta - \beta_c$, we find from expanding Eq. (10) that

$$x_s - x_c = \frac{f_\beta(\beta_c, x_c)}{1 - f_x(\beta_c, x_c)} B \tag{13}$$

to first order. We then seek a solution for σ of the form

$$\sigma = i\omega + B(a + ib) + ... \tag{14}$$

After inserting (14) into Eq. (12), we obtain from the real and imaginary parts two equations for a and b which we solve. The real part a is given by

$$a = f_x \left[f_{xx} \frac{f_\beta}{1 - f_x} + f_{x\beta} \right] \frac{1 + \eta + (\eta\omega)^2}{(1 + \eta + (\eta\omega)^2)^2 + \omega^2 \eta^4} \tag{15}$$

where all partial derivatives are evaluated at $x = x_c$ and $\beta = \beta_c$. A stable (unstable) steady state means $Ba < 0$ ($Ba > 0$). Furthermore, a left-right change of stability ($B > 0$) is possible if $a > 0$ (forward Hopf bifurcation) and a right-left change of stability ($B < 0$) is possible if $a < 0$ (reverse Hopf bifurcation).

B. Sine-type nonlinearity

We specialize our analysis by considering the case of a sine f-function which models many optical systems producing chaos. For example, it may appear as the result of two-wave interference processes[4, 6, 13] and has the general form

$$f(\beta, x) = \beta \left[1 + C \cos(x + \Phi) \right] \tag{16}$$

where x is the dynamical variable (e.g., the optical power, an electro-optic or acousto-optic voltage, the wavelength, etc). C is a fringe contrast, Φ is a phase parameter and β is the bifurcation parameter. In most cases, experimentalists operate the optical device with a fringe contrast $C = 1$.

This is however not the case for the coherence modulation-based system studied in this paper where $C = 1/2$.

Assuming $C \leq 1$ and using (16), we evaluate the partial derivatives in (15). For large delay (η small), $f_x \simeq -1$ and the condition $a \leq 0$ simplifies as $f_{xx}\, f_\beta/2 + f_{x\beta} \geq 0$, or equivalently,

$$\beta_c^4 C^2(1-C^2) - \beta_c^2(1+2C^2) - 1 \geq 0. \tag{17}$$

Eq. (17) then implies that

$$a \;>\; 0 \text{ if } 0 < \beta_c < \beta_r \text{ (forward Hopf bifurcation)} \tag{18}$$

$$a \;<\; 0 \text{ if } \beta_c > \beta_r \text{ (reverse Hopf bifurcation)} \tag{19}$$

where

$$\beta_r \equiv \sqrt{\frac{(1+2C^2) + \sqrt{1+8C^2}}{2C^2(1-C^2)}}. \tag{20}$$

Note from (20) that $\beta_r \to \infty$ as $C \to 1$ which means that condition (19) for a reverse Hopf bifurcation cannot be verified in this case. This explain why the *"eye bifurcation cascade"* connecting a forward and a reverse Hopf bifurcation point was not observed for previous optical devices operating with C close to 1.

6. Conclusion

We reported a hybrid opto-electronic chaotic oscillator ruled by delay differential equations. The optical quantity involved in the experiment is the optical path difference of a coherence modulator. Different types of routes to chaos have been observed, from stable steady-states to chaos through periodic regimes. Two particular experimental bifurcation diagrams were presented and discussed.

Original bifurcation scenarios were reported, such as forward and reverse Hopf bifurcations. The numerical simulations are in good agreement with the experimental results. An analytical description of a specific bifurcation scenario involving forward and reverse Hopf bifurcations was proposed. The experimental setup can be used in chaos-based encryption systems with the advantage of using integrated optics technology. Another specificity of the system compared with other similar encryption devices is that the system operates with chaotic coherence-modulated light, and consequently features no detectable intensity modulation. This might offer a second level of security for information protection.

Acknowledgments

T.E. was supported by the US Air Force Office of Scientific Research grant AFOSR F49620-98-1-0400, the National Science Foundation grant DMS-9973203, the Fonds National de la Recherche Scientifique (Belgium) and the InterUniversity Attraction Pole program of the Belgian government.

References

1. Kensuke Ikeda, "Multiple-Valued Stationary State and its Instability of the Transmitted Light by a Ring Cavity System", Optics Commun. **30**, 257–261 (1979).

2. Pierre Glorieux and Albert Le Floch, "Nonlinear Polarization Dynamics in Anisotropic Lasers", Optics Commun. **79**, 229–234 (1990).

3. Henri Porte and Jean-Pierre Goedgebuer, "Bistability in Wavelength Using an Electro-Optically Tuned Dye Laser", Optics Commun. **51**, 331–336 (1984).

4. Jean-Pierre Goedgebuer, Laurent Larger, Henri Porte, and Franck Delorme, "Chaos in Wavelength with a Feedback Tunable Laser Diode", Phys. Rev. E **57**, 2795–2798 (1998); Laurent Larger, Jean-Pierre Goedgebuer, and Jean-Marc Mérolla, "Chaotic Oscillator in Wavelength : A New Setup for Investigating Differential Difference Equations Describing Nonlinear Dynamics, IEEE J. Quantum Electron. **34**, 594–601 (1998).

5. Kensuke Ikeda and M. Mizuno, "Modeling of Nonlinear Fabry-Perot Resonators by Difference-Differential Equations", IEEE J. Quantum Electron. **21**, 1429–1434 (1985).

6. J. Y. Gao, J. M. Yuan, and L. M. Narducci, "Instabilities and Chaotic Behavior in a Hybrid Bistable System with a Short Delay", Optics Commun. **44**, 201–206 (1983).

7. Jesper Mørk, Bjarne Tromborg, and Jannik Mark, "Chaos in semiconductor lasers with optical feedback: theory and experiment", IEEE J. Quantum Electron. **28**, 93–108 (1992); Toshiyuki Takizawa, Yun Liu, and Junji Ohtsubo, "Chaos in a Feedback Fabry-Pérot Interferometer", IEEE J. Quantum Electron. **30**, 334–338 (1994).

8. T. B. Simpson, J. M. Liu, A. Gavrielides, V. Kovanis and P. M. Alsing, "Period-doubling cascades and chaos in a semiconductor laser with optical injection", Phys. Rev. A **51**, 4181–4185 (1995); T. C. Newell, V. Kovanis, and A. Gavrielides, "Experimental Demonstration of Antimonotonicity: The Concurrent Creation and Destruction of Periodic Orbits in a Driven Nonlinear Electronic Resonator", Phys. Rev. Lett **77**, 1747–1750 (1996).

9. Henri Porte, Jean-Pierre Goedgebuer, Wilhelm Elflein, Albert Terras, Frédéric Le Deventec, and Nadia Butterlin, "Linear Phase Tracking in a Coherence Modulation Electrical Sensor System Using Integrated $LiNbO_3$ Modulator/Demodulator", IEEE J. of Selected Topics in Quantum Electron. **2**, 319–325 (1996).

10. Jean-Pierre Goedgebuer, Richard Ferrière, and André Hamel, "Polarization-Independent Transmission on a Single Mode Fiber Using Coherence Modulation of Light", IEEE J. Quantum Electron. **27**, 1963–1967 (1991).

11. Yuri Mazurenko, Remo Giust, and Jean-Pierre Goedgebuer, "Spectral coding for secure optical communications using refractive index dispersion", Optics Commun. **133**, 87–92 (1997); W. Wells, R. Stone, and E. Miles, "Secure commnunications by optical homodyne", IEEE J. Selected areas in Communications **11**, 770–777 (1993); Bruno Wacogne, Wilhelm Elflein, Christian Pieralli, Pascal Mollier, Henri Porte, and D. A. Jackson, "Secrecy improvement in confidential coherence modulation by means of new keying structure", Optics Commun. **154**, 350–358 (1998).

12. Jean-Pierre Goedgebuer, Henri Porte, and André Hamel, "Electrooptic modulation of multilongitudinal mode laser diodes: demonstration at 850 nm with simultaneous data trasmission by coherence multiplexing", IEEE J. Quantum Electron. **23**, 11135–1144 (1987).

13. F. A. Hopf, D. L. Kaplan, H. M. Gibbs, and R. L. Schoemaker, "Bifurcation to chaos in optical bistability", Phys. Rev. A **25**, 2172–2182 (1982); Réal Vallée and C. Delisle, "Mode Description of the Dynamical

Evolution of an Acousto-Optic Bistable Device", IEEE J. Quantum Electron. **21**, 1423–1428 (1985).

List of Figures

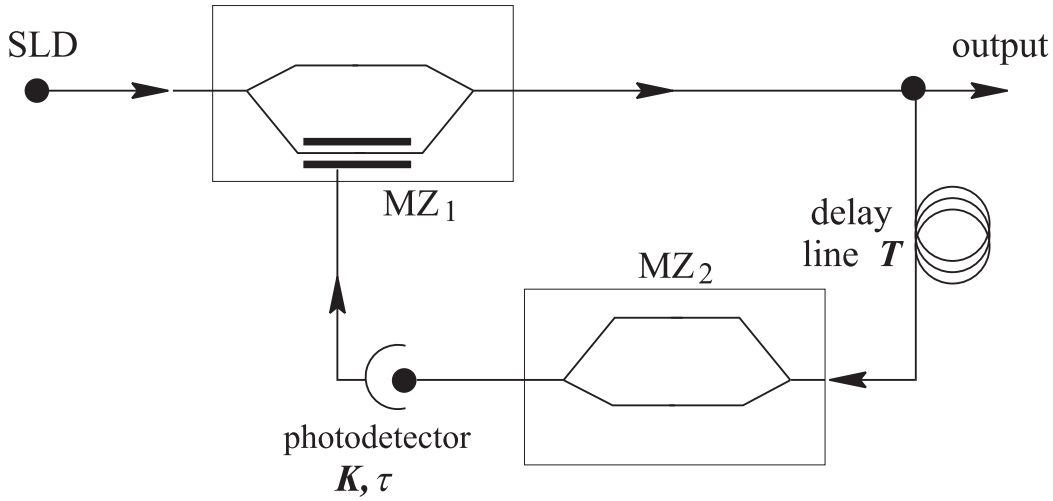

Figure 1, L. Larger et. al.

Fig. 4. Experimental bifurcation diagrams. a, $\Phi = 0$. b, $\Phi = \pi$.

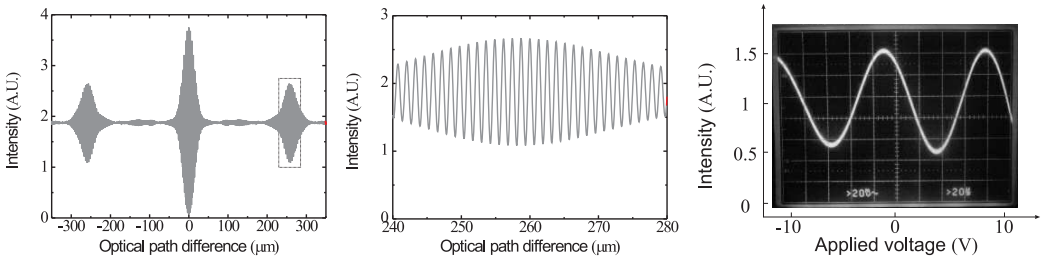

2a. 2b. 2c.

Figure 2, L. Larger et. al.

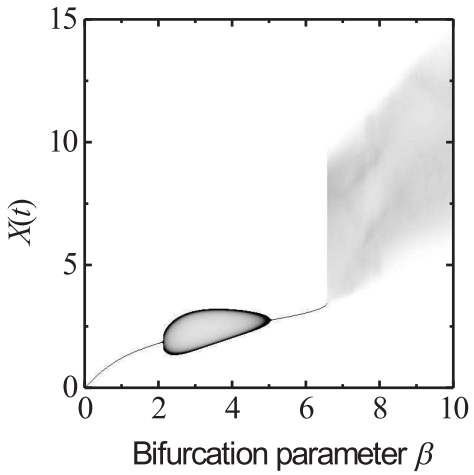

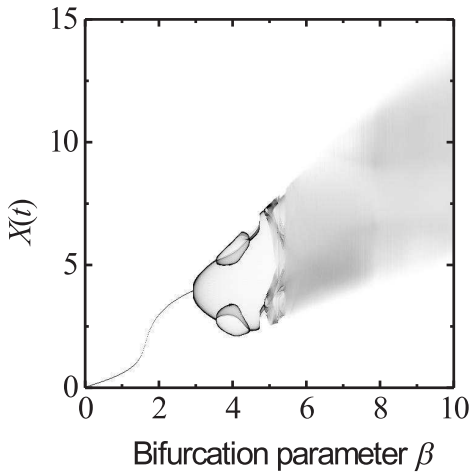

3a. 3b.

Figure 3, L. Larger et. al.

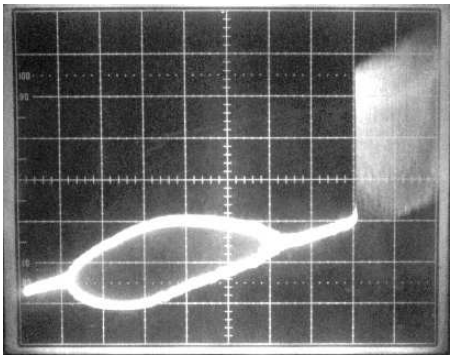

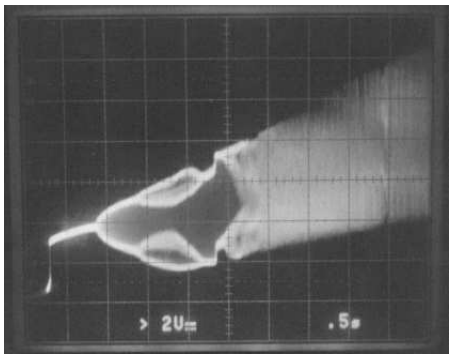

4a. 4b.

Figure 4, L. Larger et. al.